Muon Tomography sites for Colombian volcanoes

A. Vesga-Ramírez[a,b], D. Sierra-Porta[a,c,1], J. Peña-Rodríguez[a], J.D. Sanabria-Gómez[a], C. Sarmiento-Cano[a,d], M. Suárez-Durán[a,e], M. Valencia-Otero[a], H. Asorey[f,g,h,d], L. A. Núñez[a,i,2]

[a]*Escuela de Física, Universidad Industrial de Santander, 680002 Bucaramanga-Colombia.*
[b]*Centro Internacional para Estudios de la Tierra, Comisión Nacional de Energía Atómica Buenos Aires-Argentina.*
[c]*Centro de Modelado Científico, Universidad del Zulia, 4001 Maracaibo-Venezuela.*
[d]*Instituto de Tecnologías en Detección y Astropartículas, 1650, Buenos Aires-Argentina.*
[e]*Departamamento de Física y Geología, Universidad de Pamplona, Pamplona-Colombia.*
[f]*Laboratorio Detección de Partículas y Radiación, Instituto Balseiro*
[g]*Centro Atómico Bariloche, Comisión Nacional de Energía Atómica, Bariloche-Argentina*
[h]*Universidad Nacional de Río Negro, 8400, Bariloche-Argentina*
[i]*Departamento de Física, Universidad de Los Andes, 5101 Mérida-Venezuela.*

Abstract

By using a very detailed simulation scheme, we have calculated the cosmic ray background flux at 13 active Colombian volcanoes and developed a methodology to identify the most convenient places for a muon telescope to study their inner structure.

Our simulation scheme considers three critical factors with different spatial and time scales: the geomagnetic effects, the development of extensive air showers in the atmosphere, and the detector response at ground level. The muon energy dissipation along the path crossing the geological structure is modeled considering the losses due to ionization, and also contributions from radiative Bremßtrahlung, nuclear interactions, and pair production.

By considering each particular volcano topography and assuming reasonable statistics for different instrument acceptances, we obtained the muon flux crossing each structure and estimated the exposure time for our hybrid muon telescope at several points around each geological edifice. After a detailed study from the topography, we have identified the best volcano to be studied, spotted the finest points to place a muon telescope and estimated its time exposures for a significant statistics of muon flux.

We have devised a mix of technical and logistic criteria –the "rule of thumb" criteria– and found that only Cerro Machín, located at the Cordillera Central (4˚29'N 75˚22'W), can be feasibly studied today through muography. Cerro Negro and Chiles could be good candidates shortly.

Keywords: Muongraphy, Muon Tomography, Muon, Volcanoes, Cosmic Ray Techniques.

1. Introduction

Muography is a non-invasive astroparticle technique, introduced several decades ago for imaging anthropic and geologic structures, benefiting from the high penetration atmospheric muons produced in cosmic rays showers. This method offers a spatial resolution in the order of tens of meters, up to a kilometer of penetration, and measures the out-coming muon flux for different directions by means of a hodoscope. The flux variance between trajectories allows us to extract information about the inner density distribution of the scanned object. In the beginning, the study of cosmic rays –and particularly their detection after crossing geological structures– were motivated by the need to understand the background noise in particle detectors inside anthropic/natural structures [1, 2]. Luis Alvarez [3] was the first to apply muon radiography, with no results,´ to the pyramid of Cheops; but this initiative led to the successful *ScanPyramids project*, which recently discovered cavities in the Pyramid of Khufu (Cheops) [4].

The interest in muon radiography for Earth sciences studies arose after the discovery of the significant penetrating power of some high energy secondary particles produced by the interaction of cosmic rays with the atmosphere (hereafter, primaries). These particles can cross hundreds of meters of rock with an attenuation related to the amount of matter traversed along its trajectory [5]. This technique uses the same basic principles

as a standard medical radiograph: it measures, with a sensitive device, the attenuation of cosmic muons when crossing geological structures. Although there are limitations with muography in detecting deep structures beneath the volcano (such as a magma chamber), it is particularly useful when it is applied to shallow volcano phenomena such as the conduit dynamics. Thus, volcano muography constitutes a unique method to obtain direct information on the density distribution inside geological objects with a better spatial resolution than other geophysical techniques (see [6, 7, 8, 9, 10, 11, 12, 13, 14, 15, 16, 17, 18], and references therein).

Colombia, located in the Pacific Belt, has more than a dozen active volcanoes (see figure 1) clustered in three main groups along the Cordillera Central, the highest of the three branches of the Colombian Andes. Most of these volcanoes represent a significant risk to the nearby population in towns and/or cities [19, 20, 21] and have caused major disasters. The most recent, the Armero tragedy occurred in November 13, 1985, when pyroclastics of the Nevado del Ruiz fused about 10% of the mountain glacier, sending lahars with the terrible, devastating result of 20,000 casualties [22].

Therefore, to determine and to model the inner volcano structure is crucial in evaluating its potential risks. Muon tomography is a powerful technique, which measures the cosmic muon flux attenuation by rock volumes of different densities, allowing the projection of images of volcanic conduits at the top of the volcanic edifice. It constitutes an attractive way to infer density distributions inside different geological structures, which is critical in the study of possible eruption dynamics associated with specific eruptive styles. Nowadays, astroparticle research groups in Colombia have started to explore this technique to estimate the density distribution within geological edifices by recording the variation of the atmospheric muon flux crossing the structure [23, 24, 25, 26, 27, 28, 29].

The objective of the present work is twofold: first, to identify possible muon telescope observation sites to study Colombian active volcanoes by estimating the muon flux emerging from the geological edifices and second, to determine the time exposure for our hybrid muon telescope at those selected sites. Section 2 describes four of the main active Colombian volcanoes. In Section 3, we discuss the detailed simulation scheme used to estimate the incoming atmospheric muon flux and, we also investigate the energy loss of muons crossing the volcano edifice. For completeness, our hybrid muon telescope is briefly described in section 4. In 5, we analyze muon propagation across the Machín volcano and calculate the exposure times for four observation points. We also estimate the outgoing muon flux from the geological structures that could be detected by our telescope. Besides, this Section discusses a ray-tracing analysis for muon propagation at three other active volcanoes: Chiles, Cerro Negro, and Galeras.

From the previous results we devise in Section 6 "rule of thumb" criteria that should be fulfilled by the potential sites (listed below) and apply them to 13 active Colombian volcanoes. Finally, in Section 7 conclusions are presented along with possible future works.

2. Volcanoes in Colombia

In this work, we have considered 13 Colombian active volcanoes: Azufral, Cerro Negro, Chiles, Cumbal, Doña Juana, Galeras, Machín, Nevado del Huila, Nevado del Ruíz, Nevado Santa Isabel, Nevado del Tolima, Puracé, and Sotará. Figure 1 displays an artistic representation of their geographic distribution. Because of their social significance and eruptive history, we shall briefly describe some of the characteristics of four of them: Galeras, Nevado del Ruiz, Cerro Machín, and the Cerro Negro-Chiles complex.

2.1. Cerro Machín

The Machín volcano is often overlooked as a minor edifice in the Cerro Bravo-Cerro Machín volcanic belt but, considering its high explosive potential, dacitic composition and magnitude of past eruptions, it should be considered one of the most dangerous active volcanoes in Colombia [30]. It is also located at the Cordillera Central (4°29'N 75°22'W), between Cajamarca and Machín [31].

Over the last 5,000 years, Machín has had six eruptions –the last one occurred about 850 years ago– generating pyroclastic flows, depositing several tens of centimeters of ashlayers, throwing eruptive columns (several tens of kilometers) and flows of volcanic mud. In recent times some of the manifestations of Machín's volcanic activity are the presence of fumaroles, permanent microseismicity, thermal waters flowing in the vicinity of the crater, geoforms of the well-preserved volcanic building and a more significant presence of Radon gas 85 in the sector [30, 32].

The Machín volcano, with a crater 2.4km in diameter and 450m high, polygenetic, has a dome –developed through hundreds of thousands or million years–, with sedimentary and morphologic characteristics that suggest a Toba cone structure, built during the most recent phreatomagmatic [33]. According to studies related to the geological history of this volcano, a future pyroclastic eruptive episode would be deposited mainly in an area

109　of 10 km^2 around the volcano edifice [34]. The similarity in the morphology of two volcanic structures and the
110　activity of one of them must be taken into account, as one more element, in the evaluation of the danger of an
111　eventual eruption. That could be the case with the similitude of the Cerro Machín Volcano and the Chichón or
112　Chichonal Volcano in southern México in the state of Chiapas (17° 21'N; 93° 41'W; 1100 m.a.s.l) [3] which
113　should alert about the potential danger of Machín volcano.
114

115
116　*Figure 1: Artistic representation of 13 Colombian active volcanoes –Azufral, Cerro Negro, Chiles, Cumbal,*
117　*Doña Juana, Galeras, Machín, Nevado del Huila, Nevado del Ruíz, Nevado Santa Isabel, Nevado del Tolima,*
118　*Puracé, and Sotará– are displayed in three disperse clusters through the Cordillera Central. Because of their*
119　*social significance and eruptive history, we shall briefly focus on four of them: Galeras, Nevado del Ruiz, Cerro*
120　*Machín and Cerro NegroChiles. Galeras, Cerro Negro-Chiles volcanoes are found in the southern cluster,*
121　*while Nevado del Ruiz and Cerro Machín are located within the most northern one.*
122
123　*2.2. Cerro Negro - Chiles*
124　100 The Chiles and Cerro Negro are located on the Colombia-Ecuador border, 86 km from the city of San Juan
125　de Pasto, at geographic coordinates 0°49'N 77°56'W and 0°46'N 77°57'W, respectively.
126　This volcanic complex lies at the intersections of three faults: Chiles-Cerro Negro, Chiles-Cumbal and Cerro
127　Negro-Nasta. The volcanic domes reach 4748 m.a.s.l (Chiles), 4470 m.a.s.l (Cerro Negro), and their craters
128　have diameters of 1.0 km and 1.8 km, respectively. These two adjacent volcanic cones are collapsed towards
129　the north (Chiles) and west (Cerro Negro), with the presence of geoforms of an already extinct glacier action.
130　Their buildings are formed mainly by several episodes of lava and pyroclastic, with main volcanic products
131　classified as andesites of two pyroxenes and olivines.

---

[3] https://en.wikipedia.org/wiki/Chichonal

3

Although there are no historical records of eruptive activity, there is evidence of highly explosive stages, and the current activity is displayed by the presence of hot springs and solfataras. On the Ecuadorian side of Chiles, there is a seismological station which detects various activity.

2.3. Galeras

The Galeras volcanic complex –located in southwest Colombia: 1°13'18.58"N, 77°21'33.86"W– is the most active volcano in Colombia with the highest social risk due to its regular activity and the populated area that surrounds it.

Surpassing 5,000 years of antiquity, this volcanic complex has a base diameter of 20 km, a summit elevation of 4,276 m.a.s.l., and a primary crater diameter of 320m. The active cone, called Galeras Volcano, rises 1600 m above and approximately 9 km away from the city of San Juan de Pasto (capital of Nariño department) with a population of 313,000 inhabitants.

Galeras is characterized by andesite lava & pyroclastic with significant fallout deposits, displaying a conical shape with a large caldera at the top. After a long period of inactivity of more than 40 years, it awoke again in 1987, experimenting mainly minor eruptions, some with explosive character: fumarolic formation and enlargement, strong tremors, shockwaves and emission of pyroclasts and ashes [35, 36]. Since 2009, the activity has been considerably reduced to the expulsion of ashes –columns that have reached 10km– and shockwaves [37].

2.4. Nevado del Ruíz

The ice-covered volcano Nevado del Ruíz (NRV), found at the Cordillera Central –4°53'N and 75°19'W– has an altitude of approximately 5390 m.a.s.l., covering an area of more than 200 square kilometers. Its main crater (Arenas) is one kilometer in diameter and 240m deep. La Piraña and La Olleta are two small parasitic edifices, and there are four U-shaped amphitheaters produced by flank collapse and fault activity [38].

This enormous volcano is located at the junction of two fault systems: the N75°W normal Villa María-Termales fault system and the N20°E right-lateral strike-slip Palestina fault system [39]. The north and northwest borders show uneven geometries caused by the location of large amphitheaters on the upper part of the volcano, the southern and southwestern fringes are marked by sharp regular slopes while the east and southeastern fringes present moderateto-strong declivities and a significant thickness of glacier deposits.

The eruptive history of the Nevado del Ruíz runs from the Pleistocene to the present, and its stratigraphy has three main stages related to the alternate construction-destruction of its edifice: Ancestral Ruiz (2-1 mega-years), Older Ruiz (0.8-0.2 mega-years) and Present Ruiz (¡0.15 mega-years) [40]. The present emplacement of lava domes is made of andesite and dacite inside older calderas [41]. During the past 11,000 years, this volcano has passed through at least 12 eruption stages, which included multiple slope failures (rock avalanches), pyroclastic and lahars, leading to the partial destruction of the summit domes [40, 41]. The eruptions of the last thousand years have mostly been small, excluding some like the phreatic-magmatic eruption on November 13, 1985, which involved the partial melting of the glacier cap and consequent lahars, which reached and destroyed the municipality of Armero-Tolima and caused a large number of casualties.

3. Muon flux simulation chain and rock opacity

3.1. Muon flux simulation chain

Particles measured at the ground level (secondaries from now on) come from a chain of interactions and reactions, started by the primaries impinging upon the outer atmosphere. The modulation of secondaries needs to be monitored and carefully corrected by taking into account atmospheric factors that could modify its flux. Thus, a complete and detailed simulation chain –considering factors such as geomagnetic conditions, atmospheric reaction and detector response– is needed to characterize the expected flux at the detector level. Any attempt to estimate the expected flux of secondaries at the detector level should consider a detailed simulation that takes into account all possible sources of flux variations of processes occurring at different spatial and time scales. We can illustrate this conceptual scheme as [42, 43, 44]:

Cosmic Ray Flux→Heliosphere Modulated Flux   → Magnetosphere   →   ⋯   →   Primaries
        →Atmosphere Secondaries   → Detector response   → Signals.

We start our simulation chain by characterizing the effects of the geomagnetic field (GMF) on the propagation of charged particles contributing to the background radiation at ground level. This is included through the

188 calculation of directional rigidity cut-off, R_c, at the detector site, determined by using the Magnetocosmics code,
189 which implements the backtracking technique [45, 46]. GMF at any point of Earth is calculated by using the
190 International Geomagnetic Field Reference [47], for modeling the near-Earth magnetic field ($r \leq 5R_\oplus$) and by
191 the Tsyganenko Magnetic Field model version 2001 to describe the outer GMF ($r \leq 5R_\oplus$) [48].
192 The second link in this chain corresponds to a detailed simulation of extensive air showers produced during the
193 interaction of the flux of primaries –from protons to irons, i.e., $1 \leq Z \leq 26$– through the atmosphere. To obtain
194 this very comprehensive secondary flux at ground level we use the Corsika code [49], with a specially tuned
195 set of simulation parameters adapted to a particular geographical site. We will display these parameters in
196 Section 5.1 for the particular case of the Machín volcano. For the hadronic model of interaction in the
197 distribution of secondaries at the level of the detector, we use QGSJET-II-04 [50] as a model, and for low
198 energies, we choose the default option, GHEISHA-2002 [51].
199 To identify possible muon observation sites in Colombia, we shall implement the previously described
200 calculation scheme only at secular geomagnetic conditions –i.e., static geomagnetic corrections– focusing on
201 the detailed calculation of the crossing muon flux and the stopping power of the volcano edifice at different
202 volcano sites. Although we have implemented this general scheme, we found that geomagnetic corrections seem
203 not to be significant for the geographical location of Colombian volcanoes, because it mainly affects low energy
204 primaries [44].
205 Finally, the detector response to the different types of secondary particles at ground level is simulated using a
206 Geant4 model [52, 53] for both the scintillator panels and the water Cherenkov detector, but this last step of the
207 simulation chain will not be considered here but will be detailed in a coming work [54, 55, 56, 57].

3.2. Directional muon rock opacity

210 The open sky flux estimations at the ground level, influenced by various environmental parameters –altitude,
211 geomagnetic corrections, solar modulation, and atmospheric variations– induce some critical features in the
212 instrument design.
213 A comparison of the open sky particle flux Φ_{os} with the flux, Φ, emerging after crossing the target provides
214 information about its density gradient. To estimate this target density gradient we define the directional rock
215 opacity as the mass density ρ integrated along the muon path L as:

$$\varrho(L) = \int_L \rho(\xi)d\xi = \bar{\rho} \times L, \tag{1}$$

219 where ξ is a characteristic longitudinal coordinate through the volcano, L is the total distance traveled by muons
220 in the rock, $\bar{\rho}$ is the average density within the volcano. In our approach, we are assuming that the trajectories
221 of muons are straight lines which are not affected by Coulomb scattering processes; therefore density
222 distributions within volcano edifices can be inferred from the variation of its flux, $\Delta = \Phi - \Phi_{os}$. A more detailed
223 calculation, including second-order effects, is being carried out and will be included in future characterizations
224 of the selected places.
225 The muon energy loss along each path can be modeled as

$$-\frac{dE}{d\varrho} = a(E) + b(E)E, \tag{2}$$

229 for each muon arrival direction considering a uniform density distribution. Here E is the muon energy; $a(E)$ and
230 $b(E)$ are functional parameters depending on the rock composition/properties and $\varrho(L)$ is the density integrated
231 along the trajectory of the muons (the opacity defined by eq. (1)). The coefficient $a(E)$ represents the energy
232 loss due to ionization, while $b(E)$ takes into account the contribution of radiative losses, mainly Bremßtrahlung,
233 nuclear interactions, and pair production. The main parameters to estimate the coefficients $a(E)$ and $b(E)$ are
234 the average ratio $<Z/A>$ between the atomic and mass numbers of the material [58, 59].

4. MuTe: Colombian Muon Telescope

237 There are three main types of detectors implemented for volcano muography: (a) nuclear emulsion detectors,
238 (b) scintillation detectors, and (c) gaseous detectors. Each one has its *pros* and *cons* as described in [8, 12]. The
239 main issue in muography of large-size objects is the flux overestimation due to the background sources such as
240 the soft component of Extended Air Showers (EAS) [60, 61] and upward-going muons [10]. Here, we shall
241 present a new hybrid Muon Telescope (MuTe), combining the facilities of a hodoscope with a water Cherenkov
242 detector (WCD) in order to solve that drawback. The hodoscope estimates the event flux per trajectory

243 depending on the fired pixels in the front and the rear panel. A Time-of-Flight, ToF, system measures the time
244 taken by the crossing particles subtracting the nano-scale time stamp recorded in both panels. The WCD senses
245 the Cherenkov photons generated in the water due to the interacting charged particle. The recorded photon yield
246 is equivalent for the energy loss.
247
248 *4.1. The instrument*
249 Just for completeness, the muon telescope is briefly described to determine its acceptance so as to estimate the
250 time exposure of the instrument at the
251 245 observational sites. A detailed description of the instrument capabilities will be discussed shortly elsewhere
252 [56, 57].
253 MuTe combines two detection techniques: a hodoscope formed by two detection planes of plastic scintillator
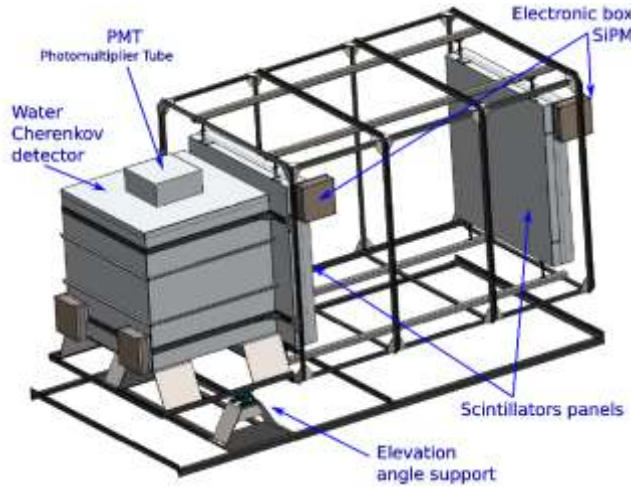254 bars, and a WCD, in an innovative setup which differentiates it from some previous detectors.
255

256
257 Figure 2: A sketch of our Colombian Muon Telescope (MuTe), which combines the facilities of a two-panel-
258 hodoscope (900 pixels) and a 1.73 m3 water Cherenkov detector.
259
260 • **Scintillators panels:** Inspired by the experiences of other volcano muography experiments [62, 63], we have
261 designed two X-Y arrays of 30×30 plastic scintillating strips (120cm×4cm×1cm), made with Styron^{TM} 665W
262 polystyrene doped with a mixture of liquid organic scintillators: 1% of 2,5-diphenyloxazole (PPO) and 0.03%
263 of 1,4-bis (5-phenyloxazol-2-yl) benzene (POPOP). Each array has 900 pixels of 4 cm×4 cm = 16 cm^2, which
264 sums up 14,400 cm^2 of detection surface which can be separated up to $D = 250$ cm (see figure 2).
265 • **Water Cherenkov Detector:** The WCD is a purified water cube of 120 cm side, located behind the rear
266 scintillator panel (again, see figure 2), which acts as an absorbing element and as a third active coincidence
267 detector. Due to its dimensions and location, it filters most of the background noise (low energies electrons,
268 protons, and muons moving backward) which could cause overestimation in the hodoscope counts [64], and it
269 is capable of isolating the muonic component of the incident particle flux. From the charge histogram, obtained
270 by time integration of the individual pulses measured in the WCD, it is possible to separate two components of
271 the incident flux: electromagnetic part (photon, electron & positron) and the $\mu-$component [42].
272
273 Muon generated events deposited in an energy range of (144MeV$ < dE/dx < $270 400MeV), represent only about
274 40% of the WCD-hodoscope acquired events. The other 60% of data is composed by ($e^{\pm}$) events under 144MeV
275 and multiparticle events above 400 MeV. Subsequently, low-momentum muons (< 1 GeV/c), which are
276 scattered by the volcano surface, are measured with a velocity of > 0.3 m/ns.
277 The Colombian MuTe combines particle identification techniques to discriminate noise background from data.
278 It filters the primary noise sources for muography, i.e., the soft-component ($e^{\pm}$) of Extensive Air Showers (EAS)
279 and scattered/upward-coming muons. Particle deposited energy identifies Electrons/positrons events in the
280 WCD, while scattered and backward muons are 280 rejected using a pico-second Time-of-Flight system.

281

4.2. Telescope acceptance

The acceptance of the instrument is a convolution of the telescope geometry (number of pixels, pixel size, and panel separation) and it is obtained multiplying the detection area by the angular resolution, i.e.

$$\mathcal{T}(r_{mn}) = S(r_{mn}) \times \delta\Omega(r_{mn}),$$ (3)

where r_{mn} represents each discrete muon incoming direction, which for an array of two panels with $N_x \times N_y$ pixels we can identify $(2N_x-1)(2N_y-1)$ different particle trajectories [17]. Moreover, the number of incident particles $N(\varrho)$ can be expressed as

$$N(\varrho) = \Delta T \times \mathcal{T} \times I(\varrho),$$ (4)

and $I(\varrho)$ is the integrated flux (measured in $cm^{-2}\,sr^{-1}\,s^{-1}$), $\mathcal{T}$ represents the acceptance (measured in $cm^2\,sr$) and ΔT designates the time exposure (in seconds). It is possible to obtain a simple relationship between the exposure time and the desired opacity resolution as

$$\Delta T \times \mathcal{T} \times \frac{\Delta I^2(\varrho_0, \delta\varrho)}{I(\varrho_0)} > c,$$ (5)

with $\Delta I^2(\varrho_0, \delta\varrho)$ the flux variation due to the different opacities ϱ_0 and $\varrho_0 + \delta\varrho$ and c is a parameter measuring the confidence level in terms of the standard deviation of the measurement. The above expression gives a bound for the minimum exposure time needed to distinguish opacity differences across the geological object [17].

In figure 3 the angular resolution and the acceptance function for our telescope (with 900 pixels and 3481 discrete r_{mn} directions) is shown. The total angular aperture of our telescope is roughly 582 mrad with the maximum point at 1.6×10^{-3} sr and, as expected, the largest detection surface corresponds to the normal direction r_{00}, reaching $\approx 6 cm^2\,sr$.

5. Machín, Chiles, Cerro Negro and Galeras Volcanoes

In this Section we shall first present a detailed study of the muon propagation across the Machín volcano and calculate the corresponding exposure times for four observation points. We shall also display estimations of the outgoing muon flux from the Machín dome that could be detected by our muon telescope.
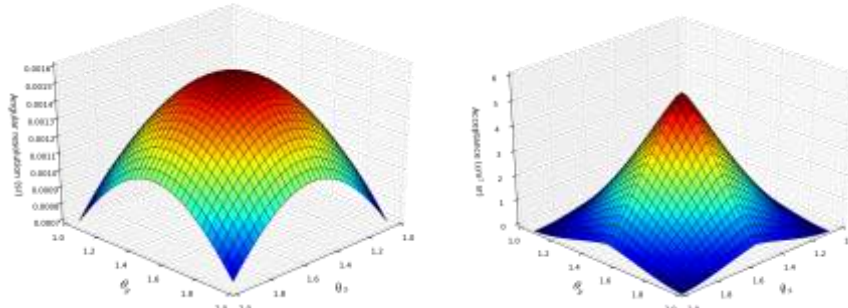

Figure 3: Angular resolution (sr) and acceptance function ($cm^2\,sr$) of MuTe. Each detection panel has $N_x = N_y = 30$, 4-cm wide scintillator bars, shaping 900 pixels of $16 cm^2$ of detecting area. For this number of pixels there are 3481 discrete r_{mn} possible incoming directions.

Secondly, we also display a ray-tracing analysis for muon propagation for three other active Colombia volcanoes: Chiles, Cerro Negro, and Galeras.

From the information gathered, we identify some critical parameters that could limit the application of muography in Colombian inland volcanoes and devise a "rule of thumb" criteria to identify possible muography volcano candidates.

5.1. Detailed study of the flux from the Machín volcano

We start our study with Machín volcano because it is one of the most dangerous active volcanoes in Colombia. It has an average height of 2750m.a.s.l; a crater of 2.4km of diameter blended into the landscape of its nearby topography, which makes it practically invisible. This fact increases the risk of the Machín volcano for the

326 surrounding population. Additionally, the morphological similarities between Chichonal and Machín volcanoes
327 –both are considered stratovolcanoes and went unnoticed as volcanoes for decades [65, 66]– is impressive. The
328 resemblances of these two volcanic buildings amaze and, the chipping of the eruption of the Chichonal volcano
329 –the largest in the history of México, with an affectation of almost 100km around– should alert about the
330 potential danger of Machín.
331 We implement the simulation chain described in section 3.1 to estimate the spectral composition of the open
332 sky particle flux, Φ_{os}, at the top of Machín volcano (4°29'N 75°22'W). Figure 4 displays the expected
333 momentum spectra for the open sky flux of secondaries at the geographic coordinates of Cerro Machín. Notice
334 that the angular integrated flux is dominated by muons, which could reach momentums up to 10 TeV/c but with
335 the low occurrence, while the most probable muons arrive on average with an energy of 4GeV/c.
336 The Corsika simulations executed at the top of Machín volcano, have the following set of parameters: Latitude:
337 4.48N, Longitude: -75.39W; Magnetic Field: North $B_X = 26.91\mu$T and vertical $B_Z = 14.37\mu$T,
338 (https://www.ngdc. 325 noaa.gov/geomag/calculators/magcalc.shtml#igrfwmm); Flux time: 24h=86400s;
339 Arriving altitude: 2450m.a.s.l.; total number of simulations corresponds to 57.75 days. The zenith incidence of
340 primaries are between 0° and 90° (all range) and the primary energies (90% of protons and 10% other heavier
341 nuclei) are in the range of 5GeV and 10^6 GeV. We also select the "tropical US Standard" atmospheric model, a
342 volumetric detector for flux calculations, standard energy cuts and rigidity cutoff.
343 Next, we calculate the differential flux of muons at the above mentioned four observational points as a function
344 of the direction of arrival and determine the maximum possible depth that can be observed from each point.
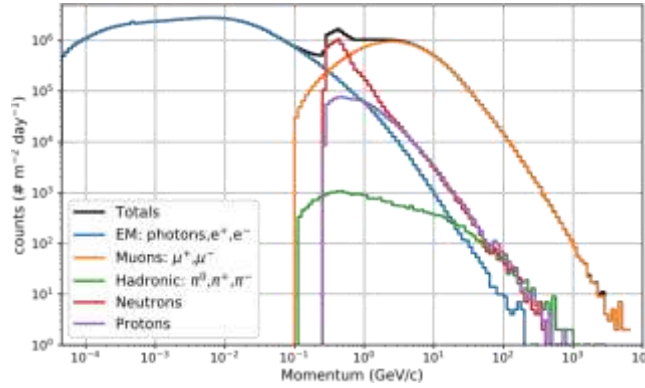345

346
347 Figure 4: The integrated spectrum of secondaries at the top of Cerro Machín. At the highest momentum of the
348 background, the flux is dominated by muons. It is noticeable that muons could reach momentums up to 10
349 TeV/c but with low occurrence, while the most probable muons arrive on average with an energy of 4GeV/c.
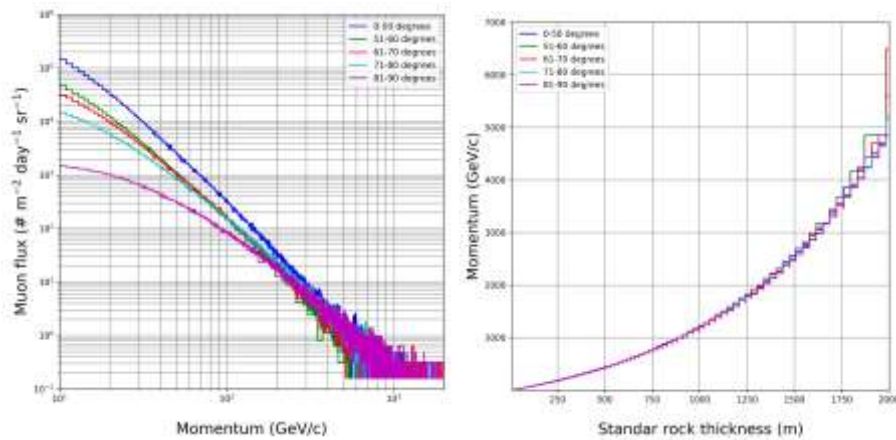350

351
352 Figure 5: Left plate displays the momentum spectra for muons emerging in five angular bins after crossing a
353 variable standard rock with density 2.65 g/cm³, measured at the point $\mathbf{P}_{1M}$ of Cerro Machín volcano. At $p_\mu \simeq$
354 500GeV/c, the integrated flux is 1cm⁻² sr⁻¹ day⁻¹ and, as expected, muons with zenith angles close to the
355 horizontal decrease by a factor of 100 with respect to those with more vertical angles of incidence. Right plate
356 illustrates the muon energy needed to cross standard rock (2.65g/cm³) thickness.

8

357

358 This is shown in the left plate of figure 5, where we display the momentum spectra for muons emerging in five
359 angular bins after crossing a standard variable rock with density 2.65 g/cm^3, measured at the point $\mathbf{P}_{1M}$ of Machín
360 volcano. As it can be clearly appreciated, the muon flux decreases considerably reaching $1\,\text{cm}^{-4}\,\text{sr}^{-1}\,\text{day}^{-1}$ for
361 $p_\mu \simeq 500\,\text{GeV/c}$.
362 We have employed the topography from the NASA Shuttle Radar Topography Mission global digital elevation
363 model of the Earth[2], with resolution of 90m×90m (see left plate in figure 6 for the particular case of the Machín
364 volcano). Next, we calculate all the possible distances crossed by each muon path integrating equation (2) and
365 (1) for standard-rock-model dome, with the coef345 ficients $a(E)$ and $b(E)$ obtained from the Particle Data
366 Group[5].
367 At Cerro Machín we have identified four observation points: $\mathbf{P}_{1M}$, $\mathbf{P}_{2M}$, $\mathbf{P}_{3M}$ and $\mathbf{P}_{4M}$ around it (see Table 1).
368 Figure 6 displays the ray-tracing technique implemented for those points with the corresponding muon
369 propagation distance through the topography, as well as the angular distribution of these distances around the
370 upper part of the volcano. Emerging muons with these trajectories have crossed about 600 meters of rock within
371 the geological structure.

372

Cerro Machín points	P1M	P2M	P3M	P4M
Latitude (°N)	4.492298	4.491984	4.487338	4.494946
Longitude (°W)	-75.381092	-75.380085	-75.379510	-75.388110
Distance to edifice center (m)	836	946	762	730
Maximum observed depth (m)	208	228	250	190

373 Table 1: Feasible observation points at Cerro Machín volcano (4°29'23.08"N, 75°23'15.39"W). The maximum
374 observed depth are those points where the emerging muon flux is less than 10^{-2} muons per cm^2 per day,
375 corresponding to zenith angles $\theta \approx 82°$.

376

377 Figure 7 displays results of 57.75 days muon flux, emerging from the volcano, and measured at the observation
378 points by our 30×30 pixels telescope with an inter-panel distance of 200cm. We have set a minimum threshold
379 count of 100 muons/pixel. Comparing figures 6 and 7, we appreciate that there are regions where the incoming
380 muon flux is highly absorbed due to the volcano geometry and the long distances traveled by these muons
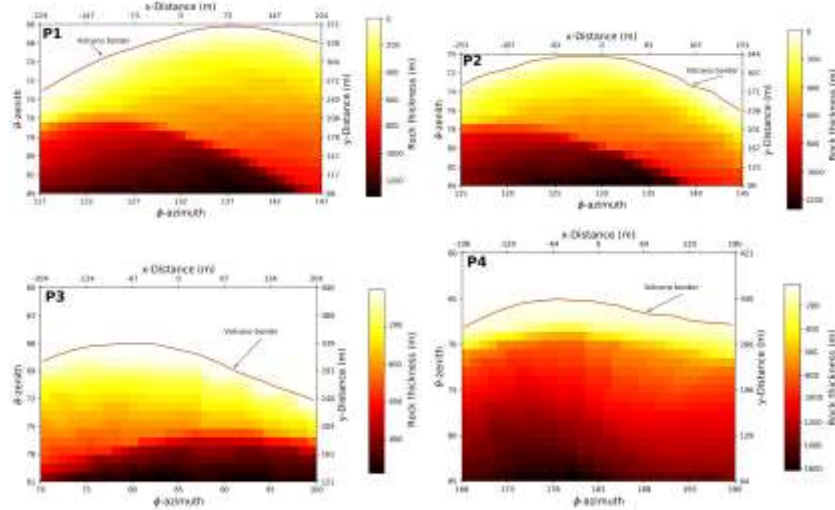381 within the volcano could easily exceed 900 meters.

382

383
384 Figure 6: Particle trajectories crossing Cerro Machín volcanic structure to the observation points $\mathbf{P}_{1M}$, $\mathbf{P}_{2M}$, $\mathbf{P}_{3M}$
385 and $\mathbf{P}_{4M}$. Notice, for example, that for $\mathbf{P}_{1M}$ observation point, muons with zenith angles $\theta > 70°$ travel distances
386 exceeding 900 meters. The topography was obtained from NASA Shuttle Radar Topography Mission global
387 digital elevation model of Earth, with SRTM3 resolution 90m×90m.

[4] See: http://www2.jpl.nasa.gov/srtm/

[5] Tables on: http://pdg.lbl.gov/2011/AtomicNuclearProperties/

388
389 We have found that very few muons –the most penetrant component of the particle shower, ranging from tenths
390 to few thousands of GeV/c–, $\approx 10^{-1}$ muons per square meter, per day, (see figure 5, left plate)– can cross almost
391 1,000m of standard rock (see figure 5, right plate or figures 6). Therefore we set 1,500m as the upper bound
392 for distances that can be traveled by the most energetic horizontal (Zenith angles & 70 degrees) muons at any
393 Colombian Volcano. Our analysis concludes that starting from a few GeV/c there is no significant effect of the
394 geomagnetic correction on the muon flux at any geographical zone in Colombia, but this correction is, in
395 general, essential to determine all the possible particle background flux at other sites with different latitudes
396 [44].
397 As we have mentioned above, we set a minimum flux of 100μ/pixel and by using equation (4) we estimate the
398 minimum time exposure needed to examine the inner structures of the volcano edifice. In figure 8 we sketch
399 contour lines representing the exposure times required, depending on the point of observation. If we assume an
400 acceptance of 6 cm^{-2} sr., we will need at least 100 days (~ 375 three months) to explore a depth of $150 - 160$
401 meters.
402 As explained before, exposure times, opacity (directional average density) and instrument resolution are related
403 through equation (5) [17]. This is another variable: the expected exposure times needed to resolve average
404 density differences of $\approx 10\%$, are shown in figure 9, for the zenithal range $66° < \theta < 84°$.
405
406 *5.2. Ray-tracing for Chiles, Cerro Negro and Galeras*
407 The idea in this Section is to look for potential observation points where the muon flux travel distance, inside
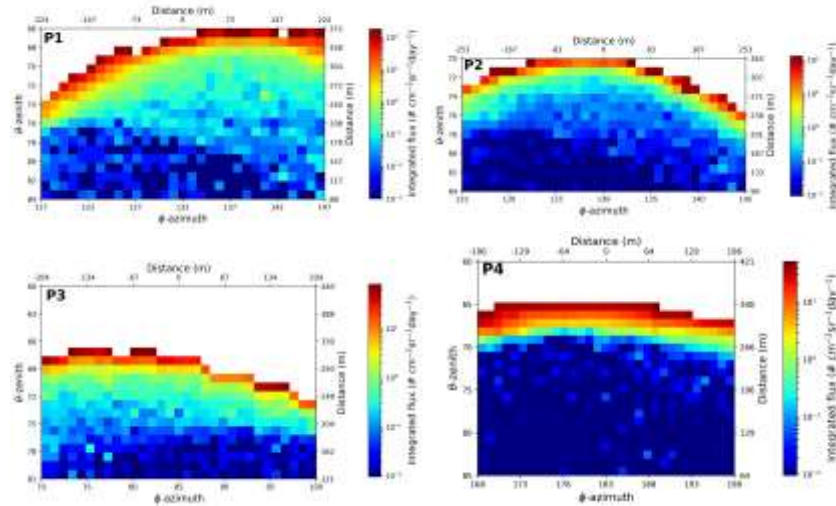408 the geological structures, is less than 1,500m.

409
410 Figure 7: Expected muon flux at $\mathbf{P}_{1M}$, $\mathbf{P}_{2M}$, $\mathbf{P}_{3M}$ and $\mathbf{P}_{4M}$ observation points in Cerro Machín, as a function of the
411 direction of incidence. Integrating equation (2) we obtain that muons with energies from 0.1 GeV/c to 10 TeV,
412 generate feeble flux:$\approx 10^{-2}$ muon per square centimeter per day at the maximum possible observed depth at
413 zenith angles $\theta \approx 81°- 84°$. White pixels represent open sky muon flux; other colors illustrate the emerging
414 muon flux from the volcano edifice. Comparing this with the previous figure, we can observe that very few
415 muons can cross the structure with traveling distances higher than 1000m.
416
417 It should be emphasized that almost all Colombian inland volcanoes are sur385 rounded by other geological
418 structures that screen the atmospheric muon flux. Thus only a few potential observation points are available.
419 We examine the other three critical Colombian volcanoes using the raytracing technique based on the
420 topography, already mentioned, above of the NASA global digital elevation model. First, the code returns the
421 latitude and longitude coordinates in vectors within a matrix of elevation values and redefines the reference
422 system (decimal degrees) to a local reference system (meters). Then we trace the muon trajectory considering
423 in detail the topography around each volcano.
424

5.2.1. Observation points at Chiles and Cerro negro volcanoes
426 At Chiles we have identified four points (see Table 2) and in figure 10 we can see the ray-tracing technique
427 implemented for $\mathbf{P}_{1Ch}$, $\mathbf{P}_{2Ch}$, $\mathbf{P}_{3Ch}$ and $\mathbf{P}_{4Ch}$ to determine the distances of muon propagation through the volcano,
428 as well as the angular distribution of these rays around the upper part of the volcano.
429 Although the distances traveled by the muons to the four observation points are less than 1,500 m, the volcano
430 was discarded due to the difficult access to these points.
431 In the case of Cerro Negro we have identified four points around it (see Table 3). In figure 11 we can see the
432 ray-tracing technique implemented for $\mathbf{P}_{1CN}$, $\mathbf{P}_{2CN}$, $\mathbf{P}_{3CN}$ and $\mathbf{P}_{4CN}$ to determine the distances of muon propagation
433 through the Cerro Negro volcano, as well as the angular distribution of these rays around the upper part of the
434 volcano. Notice that to obtain a reasonable muon flux the telescope should be tilted about seven degrees making
435 the depth of investigation very short.
436 Although the distances traveled by the muons measured from points P_{1CN}-P_{4CN} are less than 1,500m, this
437 volcano, as well as Chiles, are discarded due to the difficult access to their potential observation points. The
438 Chiles and Cerro Negro volcanoes are on the Colombia-Ecuador border, an intricate zone, where the safety of
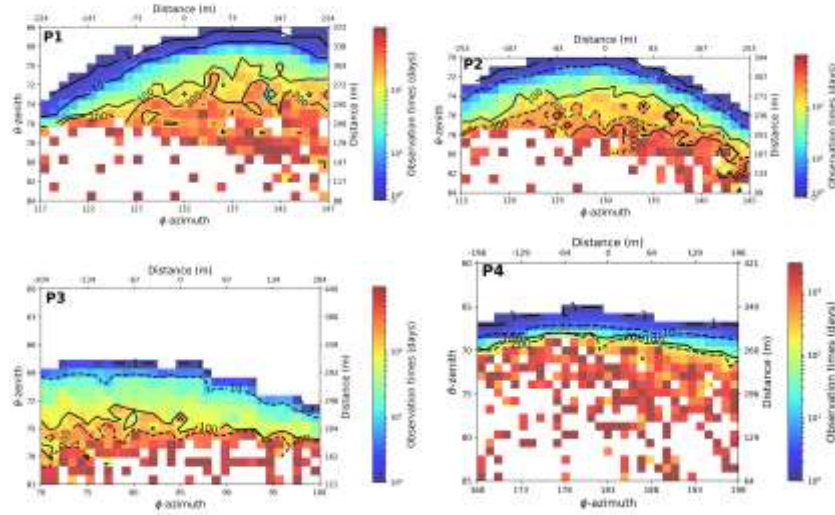439 the scientific personnel and equipment is not guaranteed by either country.
440

441
442 Figure 8: Expected observation times for 100 muons at observation points $\mathbf{P}_{1M}$, $\mathbf{P}_{2M}$, $\mathbf{P}_{3M}$ and $\mathbf{P}_{4M}$ in Cerro
443 Machín. In this calculation we assume 6cm^{-2}sr acceptance. The results agree that in order to detect 100 muons
444 in all directions an exposure time of 100 days ($\sim$ 3 months) is necessary, achieving a definition at a depth of
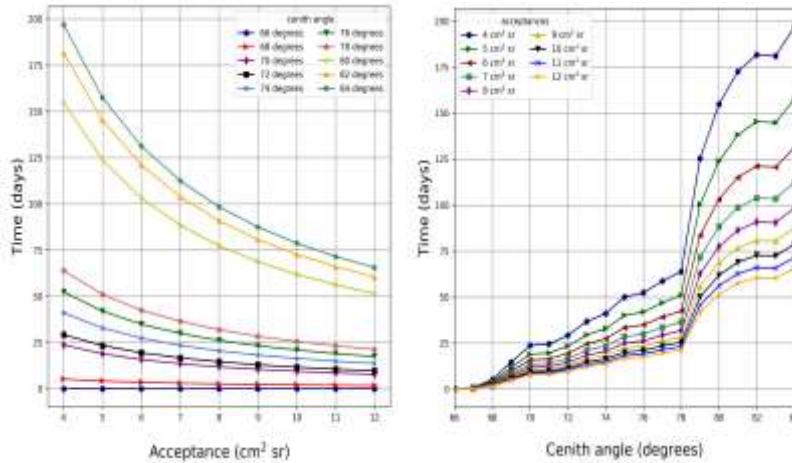445 $150 - 160$ meters.

446
447 Figure 9: Exposure times for observation point $\mathbf{P}_{1M}$ at Cerro Machín needed to identify differences of -10% in
448 the averaged directional density for different zenith angles and telescope acceptance. We obtained exposure
449 time lapses between two days and up to more than six months to achieve the desired density resolution, at
450 different zenith angles.

11

Chiles points	P1Ch	P2Ch	P3Ch	P4Ch
Latitude (˚N)	0.819431	0.823917	0.829098	0.829642
Longitude (˚W)	-77.926883	-77.927034	-77.930539	-77.933769
Distance to edifice center (m)	1050	1250	1444	1450

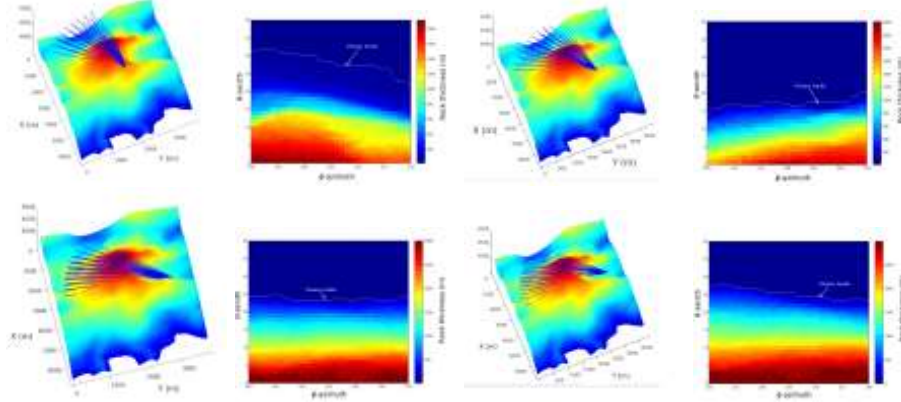Table 2: Feasible observation points at Chiles volcano (0˚49'16.32"N, -77˚56'6.13"W).

Figure 10: Particle trajectories crossing the Chiles volcano structure to observation point P_{1Ch}, P_{2Ch}, P_{3Ch} and P_{4Ch}. Points P_{1Ch} and P_{2Ch} are in areas that are difficult to access and points P_{3Ch} and P_{4Ch} in high risk areas

Cerro Negro points	P1CN	P2CN	P3CN	P4CN
Latitude (˚N)	0.826250	0.832924	0.837090	0.840811
Longitude (˚W)	-77.954136	-77.951177	-77.952412	-77.954454
Distance to edifice center (m)	1514	1912	1961	1982

Table 3: Feasible observation points at Cerro Negro volcano (4˚29'23.08"N, -75˚23'15.39"W).

5.2.2. Observation points at Galeras volcano

Galeras volcano has been active for more than a million years. Its most recent phase of activity began about 4500 years ago and included six significant eruptions. After quiescence dating from 1948, Galeras renewed its activity in 1988 with the emplacement of a dome, which was destroyed in an explosion in 1992 [67]. On January 14, 1993, an explosion in Galeras crater killed six visiting scientists and three tourist [68].

The Galera's intense activity and its proximity to an important city, generate a significant interest to study this Volcano with all techniques available and muography do not escape from this pressure. Several local researchers have made a notable effort in modeling muon transport properties across this dangerous volcano [23, 27, 28], and some of them even proposed a design for a muon telescope [27]. It is not clear which are the geographical coordinates where they intend to place the instrument and what will be the typical exposures times so as to have statistically reasonable counts.
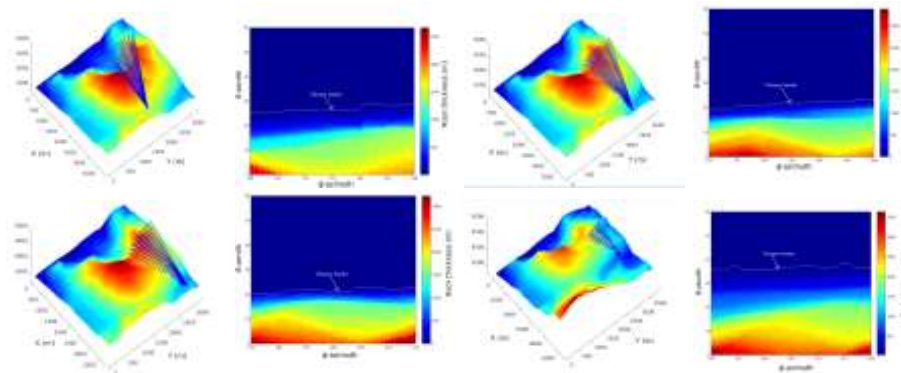
Figure 11: Particle trajectories crossing the Cerro Negro volcanic structure to the observation point **P**1*CN*, **P**2*CN*, **P**3*CN* and **P**4*CN*.

We have proceeded to identify where safe observation points might be to install our MuTe, and how long would it takes to obtain a valuable density distribution. Following this procedure, we have identified four points around Galera Volcano (see Table 4 and figure 12). However, all are in the high volcanic risk area, and so located that the detected muons through the amphitheater and 435 crater overlap, making difficult the analysis (see figure 13.

Galeras points	**P**1*G*	**P**2*G*	**P**3*G*	**P**4*G*
Latitude (˚N)	1.228158	1.223786	1.216328	1.209212
Longitude (˚W)	-77.365237	-77.362778	-77.358964	-77.363168
Distance to edifice center (m)	975	494	540	1482

Table 4: Feasible observation points at Galeras volcano (1˚13'16.02"N, 77˚21'33.09"W).

Figure 12: Feasible observation points at Galeras volcano (1˚13'16.02"N, 77˚21'33.09"W).
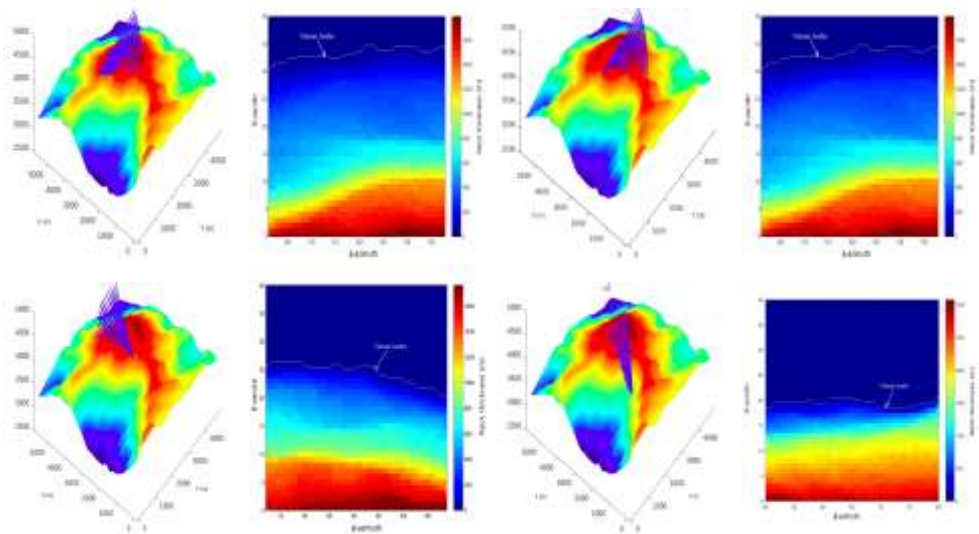

Figure 13: Particle trajectories crossing Galeras volcanic structure to the observation point $\mathbf{P}_1G$, $\mathbf{P}_2G$, $\mathbf{P}_3G$ and $\mathbf{P}_4G$.

6. Volcano observation site determination criteria

Based on the detailed analysis of the Machín volcano, and the ray-tracing studies of the Cerro Negro-Chiles complex and Galeras, we have devised a "rule of thumb" criteria to select the tentative muography observation sites of Colombian volcanoes.

These criteria for determination of the muon observation sites for the Colombian mainland volcanoes, – surrounded by other geological structures that could screen the atmospheric muon flux and having insecure access to various regions because of the internal conflict– is qualitatively different from those made on peaceful islands with volcanoes free from the screening of other mountain systems. Thus, to determine muon observation points for active volcanoes in Colombia, we have devised a mix of technical and logistic criteria, which we call the "rule of thumb" criteria that should be fulfilled by the potential sites and which are listed below:

• **Criterion 1: At the observational level, is the volcano base width less than** 1,500**m?** This criterion is necessary because the energy of atmospheric horizontal muons are two orders of magnitude lower than vertical muons and, these incident particles need two more orders of magnitude to cross the volcanic structure [64]. Therefore, most energetic horizontal muons can only cross 1,500m of standard rock, and the horizontal line of sight from the tentative observation point should be less than this distance. This criterion can be appreciated quantitatively for trajectories/flux in the case of Machín volcano (figures 6 and 7), where only few (the most energetic and horizontal) muons can cross the structure while 460 traveling distances greater than 1,500m.

• **Criterion 2: Are there tentative observation points where the surrounding topography does not interfere with the target?** Muons impacting the telescope should cross only the structure under study. Nearby mountains and any other geological formations neighboring the target volcano, must not contribute to the opacity. This requisite imposes a severe restriction on the tentative view points for the few observational places where a small window is present, with no mountains or other screening geological structures.

• **Criterion 3: Are the sites accessible and secure?** Sites must be easily accessible, and the telescope should be securely transported and placed on the field. It is essential to consider: the weight and size of the assembled telescope and its parts; also the quality and accessibility of water resources in the area. Additionally, the volcano to be studied should not be cataloged in a situation of abundant activity due to the danger of volcanic products and processes associated with eruptions such as ashfall, pyroclastic materials, lahars, floods, among other risks, as well as earthquakes and landslides that may cause severe damage to instrument and personnel. Last but not least the –vanishing– internal conflict persisting in several regions of the Colombia countryside and safe access should be taken into account.

We devised these criteria based on the detailed study of Machín volcano and the ray-tracing analysis for 13 Colombian volcanoes. The results of the application of the above criteria are summarized in table 5 and lead to the conclusion that the only Colombian volcano that could be studied through muography is Cerro Machín [69]. We hope that shortly with the end of the internal conflict, Cerro Negro and Chiles will be safely accessible because they are good candidates to be studied with muography, but today they are not yet freely reachable.

7. Discussion and Conclusions

In this work, we present the first comprehensive simulation of muon flux for the Machín volcano dome. We have also carried out a ray-tracing analysis for 12 other inland volcanoes in Colombia surrounded by complex topographic environments. After a detailed study from the topography, we have identified the best volcano to be studied, spotted the finest points to place a muon telescope 495 and estimated its time exposures for a significant statistics of muon flux.

The rationale of our new approach stems from a four-step methodology:

1. **A "rule of thumb" criteria.** We have devised a mix of technical and logistic criteria –the "rule of thumb" criteria– and applied them to 13 Colombian volcanoes. We have found that only Cerro Machín, located at the Cordillera Central (4°29'N 75°22'W), can be feasibly studied today through muography. Cerro Negro and Chiles could be good candidates shortly.

2. **A unabridged simulation of open sky particle spectrum and composition.** Corsika has calculated the energy spectrum and composition of open sky secondaries at Cerro Machín and filtered them within Magnetocosmics framework, providing a detailed description of different types of particles in the MeVs to TeVs secondary energy range [42, 43].

Volcano	Criterion 1:	Criterion 2:	Criterion 3:
Azufral	N	Y	N
Cerro Negro*	Y	Y	N
Chiles*	Y	Y	N
Cumbal	N	Y	N
Dona Juana	N	Y	N
Galeras	Y	N	Y
Machín	**Y**	**Y**	**Y**
Nevado del Huila	N	Y	N
Nevado del Ruíz	N	Y	Y
Nevado Santa Isabel	N	Y	Y
Nevado del Tolima	N	N	Y
Puracé	N	Y	Y
Sotará	N	Y	N

Table 5: Which Colombian volcano can be studied by muography? The criteria discussed in section 6 has been applied to 13 Colombian volcanoes. The three questions can be summarized as: **1-** Is the volcano base less than 1,500m?; **2-** The surrounding topography does not interfere with the observation point? and, **3-** Are the sites accessible and secure? Our studies suggest that only Cerro Machín obtains three definite answers. We hope that shortly with the end of the internal conflict Cerro Negro and Chiles will be safely accessible.

3. **A detailed calculation of the emerging muon flux.** With the above open sky particle flux and precise topographical information surrounding the volcano, we have simulated the muon propagation inside the geological edifice and estimated the emerging muon flux at four different points around Cerro Machín. This was carried out integrating the energy loss equation 2, with the coefficients $a(E)$ (ionization) and $b(E)$ (radiative losses) from reference [58].

4. **An estimation of the telescope time exposure.** With the emerging muon flux, we have calculated the time exposures of the instrument for an arbitrary statistics of 100 events at each pixel and, different values of the telescope acceptance (see Figure 9).

As we have mentioned before, most of the previous muography studied volcanoes –Mount Asama [18] in Japan; Puy de Dˆome [70] in France; Mount Etna [9] in Italy; La Soufuriere [71] in Guadalupe, to mention the most relevant studies– are topographically isolated with a relatively good and accessible observation points. None are surrounded by geological structures screening the scarce high energy horizontal muons. However, Colombia –and surely all other Andean volcanoes– is very different; most of the active volcanoes are along the Cordillera Central, surrounded by higher altitudes shielding cosmic ray flux. Therefore, we developed a methodology to identify the most feasible candidates, and only Cerro Machín emerged as a possibility.

Instead of using phenomenological and pseudo-empirical formulas to estimate the background flux at the volcano site (see [18] and references therein), we proceeded to simulate its spectrum and composition, at each particular geographical location, with two standard astroparticle tools: Corsika and Magnetocosmics. We found that incident muons range from 0.1 GeV/c to 10 TeV, and the flux of high energy muons is very feeble:≈ 10 muons per square meter per day at zenith angles $\theta \approx 82° -84°$. With the above simulation as an input, and including precise topographical information, we calculate the propagation of muons through the geological edifice and determine the emerging muon flux that could be detected at several particular observation points around the volcano (see figure 6).

We have simulated more than 50 days of muon flux to estimate the minimum time needed to obtain a flux of 100 muons per pixel and found out that we require at least three months of data acquisition to explore the Machín dome (depending on the observation point) at a depth of ≈ 110m.

Then, to discriminate density variations of 10%, we evaluated time exposures for our hybrid instrument as function of the acceptance. With these preliminary simulation results and by considering the standard configuration of our telescope, we have estimated time intervals between 100 to 125 days for the upper end $(114 - 150$m$)$ of the volcano edifice.

Muography can not image deep volcano structures, but it seems to be useful in determining shallow phenomena with an excellent spatial resolution. This technique can not give direct information on when a volcano will erupt, but it could provide significant insights about possible eruption processes, in the upper end of the edifice. This emerging technique requires significant progress in data analysis, treatment and interpretation of the experimental data obtained. For a bright future, it depends on the synergy between two active international communities: particle physicists and geophysicists [12].

References

[1] E. George, Cosmic rays measure overburden of tunnel, Commonwealth Engineer 1 (1955) 455–457.

[2] A. Zichichi, O. Barnabei, P. Pupillo, F. Monaco, Subnuclear Physics: The First 50 Years: Highlights from Erice to ELN, Vol. 24, World scientific, 2000.

[3] L. Alvarez, J. Anderson, F. El Bedwei, M. Sharkawi, L. Yazolino, Search for Hidden Chambers in the Pyramids, Science 167 (3919) (1970) 832–839. doi:10.1126/science.167.3919.832. URL http://www.sciencemag.org/content/167/3919/832.extract

[4] K. Morishima, M. Kuno, A. Nishio, N. Kitagawa, Y. Manabe, M. Moto, F. Takasaki, H. Fujii, K. Satoh, H. Kodama, K. Hayashi, S. Odaka, S. Procureur, D. Attié, S. Bouteille, D. Calvet, C. Filosa, P. Magnier, I. Mandjavidze, M. Riallot, B. Marini, P. Gable, Y. Date, M. Sugiura, Y. Elshayeb, T. Elnady, M. Ezzy, E. Guerriero, V. Steiger, N. Serikoff, J.-B. Mouret, B. Charl`es, H. Helal, M. Tayoubi, Discovery of a big void in khufu?s pyramid by observation of cosmic-ray muons, Nature 552 (7685) (2017) 386.

[5] K. Nagamine, Introductory muon science, Cambridge University Press, 2003.

[6] L. F. Thompson, J. P. Stowell, S. J. Fargher, C. A. Steer, K. L. Loughney, E. M. O'Sullivan, J. G. Gluyas, S. W. Blaney, R. J. Pidcock, The application of muon tomography to the imaging of railway tunnels, arXiv e-prints (2019) arXiv:1906.05814arXiv:1906.05814.

[7] R. Kaiser, Muography: overview and future directions, Philosophical Transactions of the Royal Society A: Mathematical, Physical and Engineering Sciences 377 (2137) (2019) 20180049.

[8] H. K. M. Tanaka, L. Oláh, Overview of muographers, Philosophical Transactions of the Royal Society A: Mathematical, Physical and Engineering Sciences 377 (2137) (2019) 20180143.

[9] D. Carbone, D. Gibert, J. Marteau, M. Diament, L. Zuccarello, E. Galichet, An experiment of muon radiography at mt etna (italy), Geophysical Journal 610 International 196 (2) (2014) 633–643.

[10] K. Jourde, D. Gibert, J. Marteau, J. Bremond d'Ars, S. Gardien, C. Girerd, J.-C. Ianigro, D. Carbone, Experimental detection of upward going cosmic particles and consequences for correction of density radiography of volcanoes, Geophysical Research Letters 40 (24) (2013) 6334–6339.

[11] H. Tanaka, Subsurface density mapping of the earth with cosmic ray muons, Nuclear Physics B-Proceedings Supplements 243 (2013) 239–248.

[12] H. Tanaka, Visualization of the internal structure of volcanoes with cosmicray muons, Journal of the Physical Society of Japan 85 (9) (2016) 091016.

[13] C. Cˆarloganu, V. Niess, S. Béné, E. Busato, P. Dupieux, F. Fehr, P. Gay, D. Miallier, B. Vulpescu, P. Boivin, C. Combaret, P. Labazuy, I. Laktineh, J.-F. Lénat, L. Mirabito, A. Portal, Towards a muon radiography of the puy de dˆome, Geoscientific Instrumentation, Methods and Data Systems 2 (1) (2013) 55–60. doi:10.5194/gi-2-55-2013. URL: http://www.geosci-instrum-method-data-syst.net/2/55/625/2013/

[14] A. Portal, P. Labazuy, J.-F. Lénat, S. Béné, P. Boivin, E. Busato, C. Cˆarloganu, C. Combaret, P. Dupieux, F. Fehr, P. Gay, I. Laktineh, D. Miallier, L. Mirabito, V. Niess, B. Vulpescu, Inner structure of the puy de dˆome volcano: cross-comparison of geophysical models (ert, gravimetry, muon imaging), Geoscientific Instrumentation Methods and Data Systems 2 (2013) 47–54.

[15]   J. Marteau, D. Gibert, N. Lesparre, F. Nicollin, P. Noli, F. Giacoppo, Muons tomography applied to geosciences and volcanology, Nuclear Instruments and Methods in Physics Research Section A: Accelerators, Spectrometers, Detectors and Associated Equipment 695 (2012) 23–28.

[16] S. Okubo, H. Tanaka, Imaging the density profile of a volcano interior with cosmic-ray muon radiography combined with classical gravimetry, Measurement Science and Technology 23 (4) (2012) 042001.

[17] N. Lesparre, D. Gibert, J. Marteau, Y. Déclais, D. Carbone, E. Galichet, Geophysical muon imaging: feasibility and limits, Geophysical Journal International 183 (3) (2010) 1348–1361.

[18] H. Tanaka, T. Nakano, S. Takahashi, J. Yoshida, M. Takeo, J. Oikawa, T. Ohminato, Y. Aoki, E. Koyama, H. Tsuji, K. Niwa, High resolution imaging in the inhomogeneous crust with cosmic-ray muon radiography: The density structure below the volcanic crater floor of mt. asama, japan, Earth and Planetary Science Letters (1–2)   (2007)   104–113.   doi:https://doi.org/10.1016/j.epsl.2007.09.001.   URL: http://www.sciencedirect.com/science/article/pii/ S0012821X07005638

[19] G. Cortés, Informe de actividad volcánica segmento norte de colombia diciembre de 2016, Tech. rep., Reporte interno, Manizales, Colombia. INGEOMINAS (2016).

[20] A. Agudelo, Informe técnico de actividad de los volcanes nevado del huila, puracé y sotará, durante el periodo de diciembre de 2016, Tech. rep., Reporte Interno, Popayan, Colombia, Servicio Geológico Colombiano (12 2016).

[21] E. Muñoz, Informe mensual de actividad de los volcanes galeras,cumbal,chiles y cerro negro, las ánimas, dona juana y azufral, Tech. rep., Reporte interno, Pasto, Colombia. INGEOMINAS (2017).

[22] T. Pierson, R. Janda, J.-C. Thouret, C. Borrero, Perturbation and melting of snow and ice by the 13 november 1985 eruption of nevado del ruiz, colombia, and consequent mobilization, flow and deposition of lahars, Journal of Volcanology and Geothermal Research 41 (1-4) (1990) 17–66.

[23] A. Tapia, D. Dueñas, J. Rodríguez, J. Betancourt, D. Martínez-Caicedo, First monte carlo simulation study of galeras volcano structure using muon tomography, in: Proceedings of Science, 2016, p. 885.

[24] H. Asorey, R. Calderón-Ardila, C. R. Carvajal-Bohorquez, S. HernándezBarajas, L. Martínez-Ramírez, A. Jaimes-Motta, F. León-Carreño, J. Peña-Rodríguez, J. Pisco-Guavabe, J. Sanabria-Gómez, M. Suárez-Durán, A. Vásquez-Ramírez, K. Forero-Gutiérrez, J. Salamanca-Coy, L. A. Nu´ñez, D. Sierra-Porta, Astroparticle projects at the eastern colombia region: facilities and instrumentation, Scientia et technica 23 (3) (2018) 391–396.

[25] H. Asorey, R. Calderón-Ardila, K. Forero-Gutiérrez, L. A. Nu´ñez, J. Peña-Rodríguez, J. Salamanca-Coy, J. Sanabria-Gómez, J. Sánchez-Villafrades, D. Sierra-Porta, minimute: A muon telescope prototype for studying volcanic structures with cosmic ray flux., Scientia et technica 23 (3) (2018) 386–390.

[26] H. Asorey, R. Calderón-Ardila, K. Forero-Gutiérrez, L. Nu´ñez, J. Peña-Rodríguez, J. Salamanca-Coy, D. Sanabria-Gómez, J. Sánchez-Villafrades, D. Sierra-Porta, minimute: A muon telescope prototype for studying volcanic structures with cosmic ray flux., Scientia et technica 23 (3) (2018) 386–390.

[27] I. Guerrero, D. Cabrera, J. Paz, J. Estrada, C. Villota, E. Velasco, F. Fajardo, O. Rodríguez, J. Rodríguez, D. Arturo, D. Dueñas, D. Torres, J. Ramírez, J. Revelo, G. Ortega, D. Benavides, J. Betancourt, A. Tapia, D. Martínez-Caicedo, Design and construction of a muon detector prototype for study the galeras volcano internal structure, in: Journal of Physics: Conference Series, Vol. 1247, IOP Publishing, 2019, p. 012020.

[28] D. Torres, D. Martínez, R. Torres, A. Tapia, J. Betancourt, J. Rodríguez, D. Dueñas, D. Arturo, Galeras Volcano internal structure characterization using geological and geophysics techniques as input to muon tomography studies, in: APS Meeting Abstracts, 2019, p. Y05.002.

[29] J. Useche-Parra, C. Avila-Bernal, Estimation of cosmic-muon flux attenuation by monserrate hill in bogota, Journal of Instrumentation 14 (02) 695 (2019) P02015.

[30] G. Cortés, Estudio geológico de los depósitos de lahar asociados a la actividad eruptiva del volcán cerro machín, Tech. rep., Reporte interno, Manizales, Colombia. INGEOMINAS (2001).

[31] H. Cepeda, L. Murcia, M. Monsalve, R. Méndez, A. Núñez, Volcán cerro machín, departamento del tolima, colombia: Pasado, presente y futuro, Tech. rep., INGEOMINAS, Informe interno (1995).

[32] H. Rueda, Erupciones plinianas del holoceno en el volcán cerro machín, colombia. estratigrafía, petrografía y dinámica eruptiva, Master's thesis, Universidad Nacional Autónoma de México, México (2005).

17

695   [33] C. Aguilar Casalla, D. Piedrahita Torres, Estratigrafía del cráter y morfología del volcán cerro machín,
696   colombia, Trabajo de grado de pregrado, Programa de Geología Universidad de Caldas, Bucaramanga,
697   Colombia (2017).
698   [34] H. Murcia, M. Sheridan, J. Macías, G. Cortés, Titan2d simulations of pyroclastic flows at cerro machín
699   volcano, colombia: Hazard implications, Journal of South American Earth Sciences 29 (2) (2010) 161–170.
700   [35] M. L. Calvache, G. P. Cortés, S. N. Williams, Stratigraphy and chronology of the galeras volcanic complex,
701   colombia, Journal of Volcanology and Geothermal Research 77 (1) (1997) 5–19.
702   [36] F. G. Cruz, B. A. Chouet, Long-period events, the most characteristic seismicity accompanying the
703   emplacement and extrusion of a lava dome in galeras volcano, colombia, in 1991, Journal of Volcanology and
704   Geothermal Research 77 (1) (1997) 121–158.
705   [37] G. Cortés, J. Raigosa, A synthesis of the recent activity of galeras volcano, colombia: Seven years of
706   continuous surveillance, 1989–1995, Journal of volcanology and geothermal research 77 (1) (1997) 101–114.
707   [38] S. Sennert, Global volcanism program 2016, Tech. Rep. 10, Smithsonian Institution and US Geological
708   Survey, report on Nevado del Ruiz (Colombia), Weekly Volcanic Activity Report (2016).
709   [39] C. Borrero, L. Toro, M. Alvarán, H. Castillo, Geochemistry and tectonic controls of the effusive activity
710   related with the ancestral nevado del ruiz volcano, colombia, Geofísica internacional 48 (1) (2009) 149–169.
711   [40] J.-C. Thouret, J. Cantagrel, R. Salinas, A. Murcia, Quaternary eruptive history of nevado del ruiz
712   (colombia), Journal of Volcanology and Geother730 mal Research 41 (1-4) (1990) 225–251.
713   [41] C. Huggel, J. Ceballos, B. Pulgarín, J. Ramírez, J.-C. Thouret, Review and reassessment of hazards owing
714   to volcano–glacier interactions in colombia, Annals of Glaciology 45 (1) (2007) 128–136.
715   [42] H. Asorey, S. Dasso, L. Nu´ñez, Y. Pérez, C. Sarmiento-Cano, M. Suárez-Durán, the LAGO Collaboration,
716   The LAGO space weather program: Directional geomagnetic effects, background fluence calculations and
717   multispectral data analysis, in: The 34th International Cosmic Ray Conference, Vol. PoS(ICRC2015), 2015, p.
718   142.
719   [43] M. Suárez-Durán, Modulación de rayos cósmicos a nivel del suelo por cambios en el campo geomagnético,
720   para la colaboración lago, Tesis maestría, Escuela de Física, Universidad Industrial de Santander, Bucaramanga,
721   Colombia (2015).
722   [44] H. Asorey, L. A. Nu´ñez, M. Suárez-Durán, Preliminary results from the latin american giant observatory
723   space weather simulation chain, Space 745 Weather 16 (5) (2018) 461–475.
724   [45] L. Desorgher, MAGNETOSCOSMICS, Geant4 application for simulating the propagation of cosmic rays
725   through the Earth magnetosphere, Tech.
726   rep., Physikalisches Institut, University of Bern, Bern, Germany (2003).
727   [46] J. J. Masías-Meza, S. Dasso, Geomagnetic effects on cosmic ray propagation under different conditions
728   for buenos aires and marambio, argentina, Sun and Geosphere 9 (2014) 41–47.
729   [47] C. C. Finlay, S. Maus, C. D. Beggan, T. N. Bondar, A. Chambodut, T. A. Chernova, A. Chulliat, V. P.
730   Golovkov, B. Hamilton, M. Hamoudi, R. Holme, G. Hulot, W. Kuang, B. Langlais, V. Lesur, F. J. Lowes, H.
731   Lu¨hr, S. MacMillan, M. Mandea, S. McLean, C. Manoj, M. Menvielle, I. Michaelis, N. Olsen, J. Rauberg, M.
732   Rother, T. J. Sabaka, A. Tangborn, L. Tøffner-Clausen, E. Thébault, A. W. P. Thomson, I. Wardinski, Z. Wei,
733   T. I. Zvereva, International Geomagnetic Reference Field: the eleventh generation, Geophysical Journal
734   International 183 (2010) 1216– 760   1230. doi:10.1111/j.1365-246X.2010.04804.x.
735   [48] N. A. Tsyganenko, A model of the near magnetosphere with a dawn-dusk asymmetry 1. mathematical
736   structure, Journal of Geophysical Research: Space Physics 107 (A8) (2002) SMP 12–1–SMP 12–15.
737   [49] D. Heck, J. Knapp, J. Capdevielle, G. Schatz, T. Thouw, Corsika : A monte carlo code to simulate extensive
738   air showers, Tech. Rep. FZKA 6019, Forschungszentrum Karlsruhe GmbH (1998).
739   [50] S. Ostapchenko, Monte carlo treatment of hadronic interactions in enhanced pomeron scheme: Qgsjet-ii
740   model, Physical Review D 83 (1) (2011) 014018.
741   [51] H. Fesefeldt, Technical report pitha-85-02, Tech. Rep. 5001, III Physikalisches Institut, RWTH Aachen
742   Physikzentrum (1985).
743   [52] S. Agostinelli, J. Allison, K. Amako, J. Apostolakis, H. Araujo, P. Arce, M. Asai, D. Axen, S. Banerjee,
744   G. Barrand, F. Behner, L. Bellagamba, J. Boudreau, L. Broglia, A. Brunengo, H. Burkhardt, S. Chauvie, J.
745   Chuma, R. Chytracek, G. Cooperman, G. Cosmo, P. Degtyarenko, A. Dell'Acqua, G. Depaola, D. Dietrich, R.
746   Enami, A. Feliciello, C. Ferguson, H. Fesefeldt, G. Folger, F. Foppiano, A. Forti, S. Garelli, S. Giani, R.
747   Giannitrapani, D. Gibin, J. G. Cadenas, I. González, G. G. Abril, G. Greeniaus, W. Greiner, V. Grichine, A.
748   Grossheim, S. Guatelli, P. Gumplinger, R. Hamatsu, K. Hashimoto, H. Hasui, A. Heikkinen, A. Howard, V.
749   Ivanchenko, A. Johnson, F. Jones, J. Kallenbach, N. Kanaya, M. Kawabata, Y. Kawabata, M. Kawaguti, S.
750   Kelner, P. Kent, A. Kimura, T. Kodama, R. Kokoulin, M. Kossov, H. Kurashige, E. Lamanna, T. Lampén, V.

Lara, V. Lefebure, F. Lei, M. Liendl, W. Lockman, F. Longo, S. Magni, M. Maire, E. Medernach, K. Minamimoto, P. M. de Freitas, Y. Morita, K. Murakami, M. Nagamatu, R. Nartallo, P. Nieminen, T. Nishimura, K. Ohtsubo, M. Okamura, S. O'Neale, Y. Oohata, K. Paech, J. Perl, A. Pfeiffer, M. Pia, F. Ranjard, A. Rybin, S. Sadilov, E. D. Salvo, G. Santin, T. Sasaki, N. Savvas, Y. Sawada, S. Scherer, S. Sei, V. Sirotenko, D. Smith, N. Starkov, H. Stoecker, J. Sulkimo, M. Takahata, S. Tanaka, E. Tcherniaev, E. S. Tehrani, M. Tropeano, P. Truscott, H. Uno, L. Urban, P. Urban, M. Verderi, A. Walkden, W. Wander, H. Weber, J. Wellisch, T. Wenaus, D. Williams, D. Wright, T. Yamada, H. Yoshida, D. Zschiesche, Geant4: a simulation toolkit, Nuclear instruments and methods in physics research section A: Accelerators, Spectrometers, Detectors and Associated Equipment 506 (3) (2003) 250–303.

[53] R. Calderón, H. Asorey, L. A. Nu´ñez, L. Collaboration, Geant4 based simulation of the water cherenkov detectors of the lago project, Nuclear and Particle Physics Proceedings (2015) 424–426.

[54] A. Jaimes-Motta, Estimación de la respuesta de un detector Cherenkov de agua al fondo de rayos cósmicos en Bucaramanga(956 m s.n.m), Tesis de pregrado, Universidad Industrial de Santander (2018).

[55] A. Vásquez-Ramírez, Estimación de la respuesta generada por el detector MuTe al paso de partículas cargadas, Tesis de maestría en física, Universi805 dad Industrial de Santander (2019).

[56] H. Asorey, R. Calderón-Ardila, L. A. Nu´ñez, J. Peña-Rodríguez, J. Pisco-Guabave, J. Sanabria-Gómez, D. Sierra-Porta, M. Suárez-Durán, A. Vásquez-Ramírez, Mute: design and construction of a muon telescope for the study of the colombian volcanoes, In preparation.

[57] A. Vásquez-Ramírez, M. Suárez-Durán, J.-M. A., R. Calderón-Ardila, J. Peña-Rodríguez, J. Sanabria-Gómez, L. A. Nu´ñez, H. Asorey, The mute detector simulation response to charged particles, In preparation.

[58] J. Beringer, J. F. Arguin, R. M. Barnett, K. Copic, O. Dahl, D. E. Groom, C. J. Lin, J. Lys, H. Murayama, C. G. Wohl, W. M. Yao, P. A. Zyla, C. Am815 sler, M. Antonelli, D. M. Asner, H. Baer, H. R. Band, T. Basaglia, C. W. Bauer, J. J. Beatty, V. I. Belousov, E. Bergren, G. Bernardi, W. Bertl, S. Bethke, H. Bichsel, O. Biebel, E. Blucher, S. Blusk, G. Brooijmans, O. Buchmueller, R. N. Cahn, M. Carena, A. Ceccucci, D. Chakraborty, M. C. Chen, R. S. Chivukula, G. Cowan, G. D'Ambrosio, T. Damour, D. de Florian, A. de Gouvea, T. DeGrand, P. de Jong, G. Dissertori, B. Dobrescu, M. Doser, M. Drees, D. A. Edwards, S. Eidelman, J. Erler,V. V. Ezhela, W. Fetscher, B. D. Fields, B. Foster, T. K. Gaisser, L. Garren, H. J. Gerber, G. Gerbier, T. Gherghetta, S. Golwala, M. Goodman, B. Grab, A. V. Gritsan, J. F. Grivaz, M. Grunewald, A. Gurtu, T. Gutsche,825 H. E. Haber, K. Hagiwara, C. Hagmann, C. Hanhart, S. Hashimoto, K. G. Hayes, M. Heffner, B. Heltsley, J. J. Hernandez-Rey, K. Hikasa, A. Hoecker, J. Holder, A. Holtkamp, J. Huston, J. D. Jackson, K. F. Johnson, T. Junk, D. Karlen, D. Kirkby, S. R. Klein, E. Klempt, R. V. Kowalewski, F. Krauss, M. Kreps, B. Krusche, Y. V. Kuyanov, Y. Kwon, O. Lahav, J. Laiho, P. Langacker, A. Liddle, Z. Ligeti, T. M. Liss, L. Littenberg, K. S. Lugovsky, S. B. Lugovsky, T. Mannel, A. V. Manohar, W. J. Marciano, A. D. Martin, A. Masoni, J. Matthews, D. Milstead, R. Miquel, K. Moenig, F. Moortgat, K. Nakamura, M. Narain, P. Nason, S. Navas, M. Neubert, P. Nevski, Y. Nir, K. A. Olive, L. Pape, J. Parsons, C. Patrignani, J. A. Peacock, S. T. Petcov, A. Piepke, A. Pomarol, G. Punzi, A. Quadt, S. Raby, G. Raffelt, B. N. Ratcliff, P. Richardson, S. Roesler, S. Rolli, A. Romaniouk, L. J. Rosenberg, J. Rosner, C. T. Sachrajda, Y. Sakai, G. P. Salam, S. Sarkar, F. Sauli, O. Schneider, K. Scholberg, D. Scott, W. G. Seligman, M. H. Shaevitz, S. R. Sharpe, M. Silari, T. Sjístrand, P. Skands, J. G. Smith, G. F. Smoot, S. Spanier, H. Spieler, A. Stahl, T. Stanev, S. L. Stone, T. Sumiyoshi, M. J. Syphers, F. Takahashi, M. Tanabashi, J. Terning, M. Titov, N. P. Tkachenko, N. A. Tornqvist, D. Tovey, G. Valencia, K. van Bibber, G. Venanzoni, M. G. Vincter, P. Vogel, A. Vogt, W. Walkowiak, C. W. Walter, D. R. Ward, T. Watari, G. Weiglein, E. J. Weinberg, L. R. Wiencke, L. Wolfenstein, J. Womersley, C. L. Woody, R. L. Workman, A. Yamamoto, G. P. Zeller, O. V. Zenin, J. Zhang, R. Y. Zhu, Review of particle physics particle data group, Physical Review D 86 (1). URL http://dx.doi.org/10.1103/PhysRevD.86.010001

[59] M. Valencia-Otero, Estudio de las componentes de secundarios en cas850 cadas originadas por rayos cósmicos para aplicaciones sobre estructuras geológicas, Tesis pregrado, Escuela de Física, Universidad Industrial de Santander, Bucaramanga, Colombia (2017).

[60] L. Oláh, D. Varga, Investigation of soft component in cosmic ray detection, Astroparticle Physics 93 (2017) 17–27. doi:10.1016/j.astropartphys. 2017.06.002. URL https://doi.org/10.1016/j.astropartphys.2017.06.002

[61] R. Nishiyama, S. Miyamoto, N. Naganawa, Experimental study of source of background noise in muon radiography using emulsion film detectors, Geoscientific Instrumentation, Methods and Data Systems 3 (1) (2014) 29–39. doi:10.5194/gi-3-29-2014. URL https://doi.org/10.5194/gi-3-29-2014

[62] T. Uchida, H. K. Tanaka, M. Tanaka, Space saving and power efficient readout system for cosmic-ray muon radiography, IEEE Transactions on Nuclear Science 56 (2) (2009) 448–452.

[63] D. Gibert, F. Beauducel, Y. Déclais, N. Lesparre, J. Marteau, F. Nicollin, A. Tarantola, Muon tomography: Plans for observations in the lesser antilles, Earth, planets and space 62 (2) (2010) 153–165.

[64]   R. Nishiyama, A. Taketa, S. Miyamoto, K. Kasahara, Monte carlo simulation for background study of geophysical inspection with cosmic-ray muons, 870 Geophysical Journal International 206 (2) (2016) 1039–1050.

[]65 G. Rubio Sánchez, La erupción del 28-29 de marzo (1982) del volcán chichonal un estudio breve de su tefra, Revista mexicana de ciencias geológicas 6 (1) (1985) 48–56.

[66] J. Macías, Geología e historia eruptiva de algunos de los grandes volcanes activos de méxico, Boletín de la Sociedad Geológica Mexicana 57 (3) (2006) 379–424.

[67] M. I. Ordón, H. Cepeda, Morphological changes of the active cone of galeras volcano, colombia, during the last century, Journal of volcanology and geothermal research 77 (1-4) (1997) 71–87.

[68] D. Seidl, M. Hellweg, M. Calvache, D. Gomez, A. Ortega, R. Torres, F. B¨oker, B. Buttkus, E. Faber, S. Greinwald, The multiparameter station at galeras volcano (colombia): concept and realization, Journal of Volcanology and Geothermal Research 125 (1-2) (2003) 1–12.

[69] H. Asorey, A. Balaguera-Rojas, L. A. Nu´ñez, J. D. Sanabria-Gómez, C. Sarmiento-Cano, M. Suárez-Durán, M. Valencia-Otero, A. VesgaRamírez, Astroparticle Techniques: Colombia Active Volcano Candidates for Muon Telescope Observation Sites, in: Revista Mexicana de Astronomia y Astrofisica Conference Series, Vol. 49 of Revista Mexicana de Astronomia y Astrofisica Conference Series, 2017, pp. 54–54. arXiv:1704.04967.

[70] P. Noli, F. Ambrosino, L. Bonechi, A. Bross, L. Cimmino, R. D'Alessandro, V. Masone, N. Mori, G. Passeggio, A. Pla-Dalmau, G. Saracino, E. Scarlini, P. Strolin, Muography of the puy de dí4me, Annals of Geophysics   60   (1)   (2017)   0105.   doi:10.4401/ag-7380.   URL: http://www.annalsofgeophysics.eu/index.php/annals/ 895 article/view/7380

[71] N. Lesparre, D. Gibert, J. Marteau, J. Komorowski, F. Nicollin, O. Coutant, Density muon radiography of la soufri`ere of guadeloupe volcano: comparison with geological, electrical resistivity and gravity data, Geophysical Journal International 190 (2) (2012) 1008–1019.